Biomass prediction of *Typha latifolia* on a paludiculture site by combining structural and spectral features from UAS data

Christina Hellmann[1], Bernd Bobertz[1], Fabian Hübner[†,1], Nora Köhn[2], Jürgen Kreyling[2], Sebastian van der Linden[1]

[1] Institute of Geography and Geology, University of Greifswald, partner in the Greifswald Mire Centre, Germany
[2] Institute of Botany and Landscape Ecology, University of Greifswald, partner in the Greifswald Mire Centre, Germany

SUMMARY

Drained peatlands need to be rewetted to reduce carbon emissions. To realise this, sustainable land-use alternatives must be implemented after rewetting. Uncrewed Aerial Systems (UAS) can aid in monitoring crop growth and spatial heterogeneity in vegetation patterns, and hence contribute to improved management. We monitored *Typha latifolia* ('Typha') biomass for an 8.5 ha rewetted paludiculture site in north-east Germany using structural (digital surface model, DSM) and multispectral data (5 spectral bands and normalized difference vegetation index, NDVI) obtained by drone surveys in July, August and September 2021. We used in-situ harvests of Typha from 1 m^2 square plots as training data. Biomass for validation plots was predicted from field measurements for the respective observation dates. The DSM's and NDVI's spatial resolution (2.76 cm) were resampled to 1 m and original values aggregated into different spatial metrics (i.e., percentiles of pixel height and NDVI values). Different regression models were separately tested for the different August DSM and NDVI metrics as explanatory variables from August data. A normalised Typha fraction cover mask from the multispectral data was used to exclude non-target species. To test the model for different phenological stages, we then applied the best performing model of August to July and September. The models were compared to non-destructive biomass predictions from linear relationships between field measurements. The combination of DSM or NDVI metrics with the Typha mask captured the heterogeneity of Typha biomass well (R^2 = 0.65–0.71). Biomass overprediction for present non-target species was successfully excluded. DSM models outperformed NDVI models for dense Typha stands due to saturation of the NDVI at 500 g m^{-2} biomass. We were able to show biomass accumulation from July to August of up to 200 g m^{-2}. The September model had the lowest performance (R^2 = 0.6), due to a weakened height-biomass relation. Further, our model underestimated flower biomass. As single UAS surveys offer both structural and spectral information, UAS data will contribute to precise biomass and vegetation monitoring at high spatial resolution in upcoming rewetting efforts.

KEY WORDS: cattail, multispectral, remote sensing, rewetting monitoring, UAV

INTRODUCTION

Peatlands are ecosystems with permanently wet soils, in which anaerobic conditions result in a low decay rate of biomass. Plant material accumulates, forms peat, and thereby stores carbon (Bonn *et al.* 2016). A huge global carbon stock has been formed by peatlands, containing 450 Gt of carbon (UNEP 2022). This makes peatlands an important factor in the context of climate change. Peatlands are drained for agriculture, forestry and peat excavation worldwide (Joosten 2016), leading to environmental degradation affecting ecosystem services. As a result, drained and, hence, degraded peatlands turn from carbon sinks into sources: stored carbon is being released as CO_2 (among other greenhouse gases (GHG)) (Tiemeyer *et al.* 2016), nutrients are being discharged (Zak *et al.* 2010), habitats of endangered species are being lost (Tanneberger *et al.* 2009) and subsidence occurs due to mineralisation (Erkens *et al.* 2016). 12 % of global peatlands are drained, and although they share only 0.5 % of the global land surface, they cause 4 % of total GHG emissions due to drainage (UNEP 2022).

In Mecklenburg - Western Pomerania, a federal state in north-east Germany, where the presented study was conducted, the emissions of drained peatlands amount to almost 40 % of the total emissions of the federal state (Uellendahl *et al.* 2023). Therefore, the rewetting of drained peatlands is a key factor in mitigating climate change (Joosten 2016). New concepts for sustainable agriculture on rewetted peatlands are necessary to replace traditional agricultural schemes on drained peatlands.

Plant biomass from paludiculture, i.e., agricultural practice on peatland under permanent wet conditions (Wichtmann *et al.* 2007) may, for example, be used as fodder or in industrial production as roofing or insulation material (Wichtmann *et al.* 2007, Oehmke & Abel 2016, Geurts & Fritz 2018). By using rewetted peatlands for paludiculture, degradation will be stopped, new habitats will be provided, hydrology improves, nutrient run-off is restrained and GHG emissions will decrease in the long term (Wichtmann *et al.* 2007, Günther *et al.* 2020). 184 plant species were identified as being suitable for paludiculture (Timmermann 2003, Wichtmann *et al.* 2007, Abel *et al.* 2013, Geurts & Fritz 2018), among them *Typha latifolia* (hereinafter 'Typha'), the target species of our study.

Typha spp. are perennial and can grow under high water levels with high biomass yields (Geurts & Fritz 2018). The basal plant parts are submerged, while the long linear leaves and flowers grow above water level (helophytes) (den Hartog & Segal 1964, Heinz 2011). Plant height can reach more than two metres (Wild *et al.* 2001). Typha produces inflorescences (also referred to as flowers) with more than 100,000 diaspores (Coops & van der Velde 1995). Since they have rhizomatous growth, they can spread quickly and build dense populations within a year (Wild *et al.* 2001). Typha can cope with a wide range of environmental conditions but profits from nutrient-rich conditions increasing its shoot density and biomass (Grace 1988, Heinz 2011, Geurts & Fritz 2018, Vroom *et al.* 2018).

During the last decades, Typha has been the object of investigation of several studies that concluded it may be a promising paludiculture crop for fodder production in dairy (Pijlman *et al.* 2019), for bioenergy (Grosshans 2014) and as insulating material (Wichtmann *et al.* 2007). Research topics were usability, plant density, water level height, biomass yields, harvest date, nutrient removal potential and GHG emissions, among other things (Pfadenhauer & Wild 2001, Wild *et al.* 2001, Timmermann 2003, Vroom *et al.* 2018, Pijlman *et al.* 2019, Ren *et al.* 2019, Geurts *et al.* 2020). For instance, yields of 10–29 t dry aboveground biomass (DAGB) Typha per ha and year can be reached in the long-term (Grosshans 2014). Typha is harvested at 10–20 cm aboveground, date of harvest depends on utilisation (Närmann *et al.* 2021). Studies investigating Typha growth after rewetting showed biomass accumulation ranging from 2 to 20 t ha^{-1} depending on nutrient availability, water table depth, duration of inundation, and stand age (Timmermann 2003, Heinz 2011, Schulz *et al.* 2011, Geurts & Fritz 2018).

To prove the economic viability and the possibility of large-scale cultivation of Typha, the project Paludi-PRIMA (Putting Paludiculture into Practice: Integration - Management - Cultivation, 2019–2022) puts the application of Typha as a paludiculture crop into a socio-economic context (Greifswald Mire Centre 2020a). For this purpose, a pilot scheme of approximately 8.5 ha with Typha planting was established in north-eastern Germany. Monitoring the development of Typha and accompanying vegetation is crucial for understanding the factors influencing Typha growth and therefore biomass yields on the study site. A better understanding of these factors allows land managers to react to and enhance growing conditions.

With remote sensing data, large areas can be covered while taking spatial variability into account. Thus, biomass has been estimated based on satellite imagery for several decades and across various ecosystems (e.g., Dong *et al.* 2003, Mutanga *et al.* 2012, Ullah *et al.* 2012, Fassnacht *et al.* 2021). Wetland biomass estimation using satellite imagery was the objective of several recent studies for assessing and monitoring ecosystem productivity. 30 m Landsat 5 imagery was used in a time series analysis to map the changes in *Spartina alterniflora* biomass in a salt marsh. Wan *et al.* (2019) used Landsat 7 and 8 imagery, covering large areas but at rather low spatial resolution (15 m) for biomass estimation of four different wetland species. Räsänen *et al.* (2021) estimated biomass from 10 m Sentinel-2 imagery and 3 m PlanetScope in a tundra landscape. Wetland biomass in South Africa was estimated by Mutanga *et al.* (2012) on a high spatial scale (2 m with World-View-2), while Räsänen *et al.* (2019) used Quick-Bird (2.4 m), WorldView-2 (2 m) and WorldView-3 (1.6 m) to predict biomass in arctic tundra and peatlands.

Uncrewed aerial systems (UAS) provide data with an even higher spatial resolution at cm-scale, while nowadays often acquiring optical imagery with four to five spectral bands. While already common in the agricultural context for monitoring crop growth (Hunt *et al.* 2005, Geipel *et al.* 2016, Willkomm *et al.* 2016, Poley & McDermid 2020), biomass estimation of wetland vegetation using UAS is still relatively new: e.g., Klemas 2013, Luo *et al.* 2017, Doughty & Cavanaugh 2019, Pätzig *et al.* 2020, Doughty *et al.* 2021. Thus, biomass estimation of Typha as a paludiculture crop has so far not been an object of investigation.

The normalised difference vegetation index (NDVI) is a common proxy to predict biomass. Doughty & Cavanaugh (2019) used the UAS derived NDVI to predict the plant biomass in coastal

wetlands. However, the saturation of the NDVI for high biomass or canopy with high density can be challenging (Tucker 1977, Cunliffe *et al.* 2020). To overcome these difficulties, it is recommended to use a multi-data input combining spectral and structural information (Luo *et al.* 2017, Poley & McDermid 2020, Lu *et al.* 2022). Spectral information refers to the band combinations (e.g., blue, green, red, red edge, NIR) from which different vegetation indices (VIs) can be calculated. Structural information is based on a digital surface model (DSM) as the height of the surface (including vegetation) or a canopy height model (CHM) as the true vegetation height. Lu *et al.* (2022), for example, successfully modelled *Phragmites australis* biomass from UAS derived NDVI and canopy height (R^2 = 0.74, RMSE = 174 g m^{-2}).

Moving window analyses can account for vegetation canopy structure at small pixel sizes. The DSM or CHM can be aggregated to a lower resolution while calculating different metrics such as mean, median and maximum height values, or different percentiles, representing spatial variability (Poley & McDermid 2020). This also applies to VIs. Luo *et al.* (2017) tested different metrics from lidar point clouds and lidar intensity. They showed the best result for the combination of modified soil-adjusted vegetation index (MSAVI) and the 99th percentile of lidar height from point clouds (R^2 = 0.65, RMSE = 168 g m^{-2}) to predict biomass for *P. australis*. Using DSM metrics for biomass prediction seems promising for Typha due to its erect growth form. However, when predicting species-specific biomass, combining VIs and structural metrics might still predict biomass for non-target species, due to similar spectral or structural signatures. Therefore, strategies are needed to derive both species abundance and biomass indicators from the combined data available from common UAS.

The overarching aim of our study was to create a regularly applicable workflow that uses a combination of multispectral and structural UAS information from single drone surveys for predicting species-specific biomass. We tested different structural DSM and NDVI metrics (from aggregating pixels to 1 m²) as the main explanatory variable, while accounting for the biomass of non-target species with a Typha fraction cover mask from the multispectral UAS imagery. Biomass varies throughout the year and different growth stages may result in different biomass prediction performances since estimates depend on growth form and stage (Doughty & Cavanaugh 2019, Poley & McDermid 2020). At the same time, reliable training data for biomass prediction models may be scarce. Therefore, we tested our suggested model on UAS data from three acquisition dates.

To achieve the overarching aim and present an approach for an improved mapping of biomass production of Typha on a rewetted site over time using multitemporal and multispectral data from one single UAS, we will address the following questions: I) Can we describe Typha biomass at high accuracy using regression modelling with structural DSM or spectral NDVI metrics? II) Can the biomass prediction be improved by including a Typha fraction cover mask from multispectral image data? III) To what extent is a model combining structural and spectral information robust with regard to applicability for different observation dates, and hence for monitoring biomass development over time? To answer these questions, we trained and tested different regression models based on data from the peak of the vegetation period in August. The best model was then applied to data from July and September of the same year to test for temporal robustness. Non-destructive biomass prediction from in-situ harvests served as model validation.

METHODS

Study area

The study area 'Polder Teichweide' is located in close proximity to the town of Neukalen, Mecklenburg - Western Pomerania, Germany. It is part of the river valley Teterower Peene west of Lake Kummerow (Figure 1). The climate is temperate with annual precipitation 583 mm and mean air temperature 9.2°C during the period 1991–2020 at the nearest weather station in Teterow (Deutscher Wetterdienst 2023).

The study area covered approximately 8.5 ha and was rewetted and planted with *Typha latifolia* and *T. angustifolia* in September 2019 as part of the Paludi-PRIMA Project (Neubert *et al.* 2022). Before that time, it was drained for grazing and winter fodder production for at least two decades. In the course of rewetting in 2019, dikes were built around the study site, and ditches outside the dams were excavated to prevent surrounding grasslands from flooding. The area was levelled to 60 cm above mean sea level by machinery, resulting in a partial removal of topsoil and grass sod (Greifswald Mire Centre 2020b). In the western area, more topsoil was removed in error. A ditch stretching from north to south was filled with organic soil (Figure 1d). The peat layer is up to 5 m thick (Greifswald Mire Centre 2020b).

Plant species composition was heterogeneous and a mixture of (wet) grassland species such as *Holcus*

lanatus and *Phalaris arundinacea* and wetland/ aquatic species including *Glyceria maxima*, *P. australis* and *Carex* spp. (Seiler 2021). Major dominant species in 2021 were *Juncus articulatus* in eastern parts, *T. latifolia* in the west and in the ditches, and *P. arundinacea* in southern parts. The latter was a remnant from pre-project conditions and grew in areas where topsoil had not been removed before rewetting (Hübner 2021). *P. australis* was mainly restricted to small patches at the edges, such as the open water body in the north-western corner and a patch at the western edge. *Carex* spp. was found in patches at the south-eastern corner, associated with the second open water body. *T. angustifolia* occurred only sparsely.

Image acquisition and pre-processing

UAS surveys were conducted on a monthly basis (Table 1), always prior to invasive sampling. A DJI Phantom 4 Multispectral was used to gather

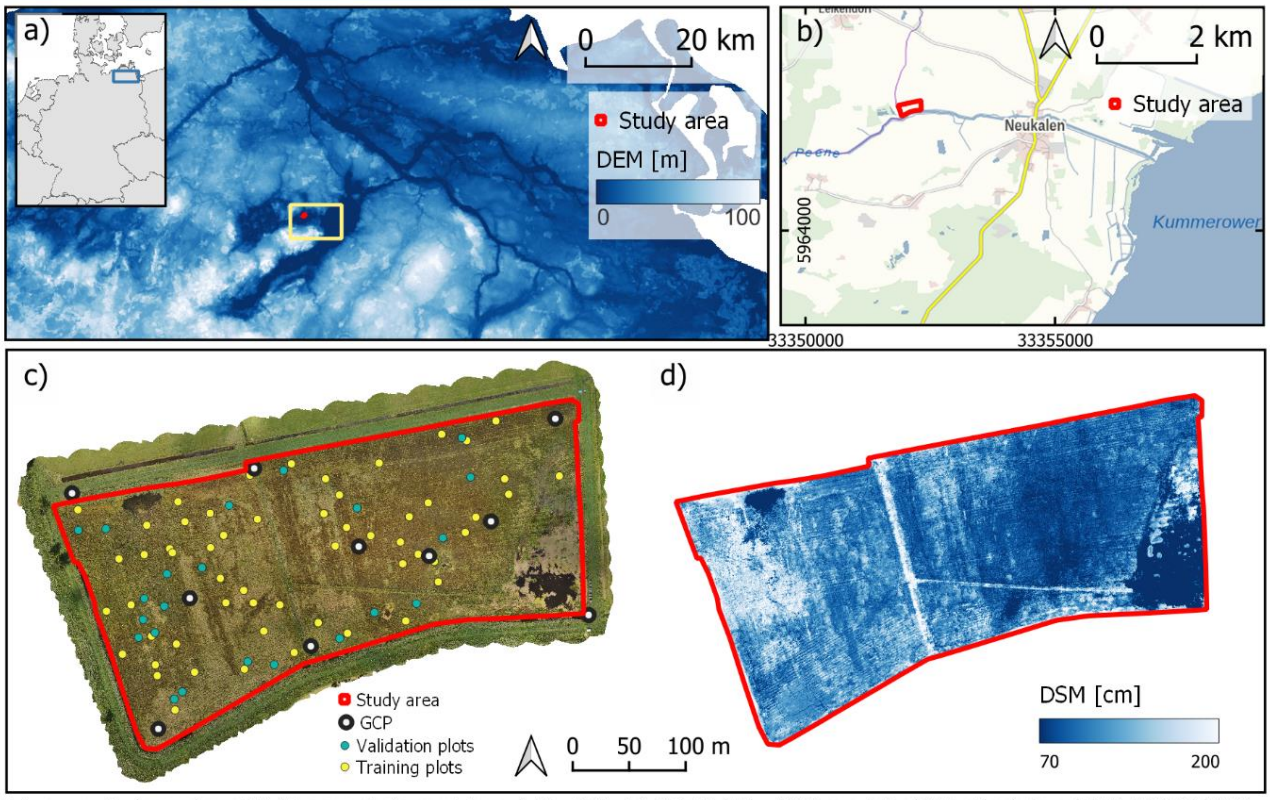

Datasources: Background map EEA (European Environment Agency). EU - DEM v1.0, EEA. WebAtlas MV. Drone derived RGB orthophoto and DSM. ETRS 89 / UTM zone 33 N.

Figure 1. a) Overview of the study area in north-eastern Germany. The altitude of the landscape surrounding the study area is generally low. The low and flat area in the eastern part of the yellow frame represents Lake Kummerow. The yellow frame indicates the extent of map b. b) The study area is adjacent to the river Teterower Peene. c) Drone derived RGB orthophoto from 03 August 2021 with Ground Control Points (GCP) training and validation plots. d) Drone derived DSM (digital surface model) from 03 August 2021. In the course of rewetting, a former ditch stretching from north to south was filled with organic soil. Vegetation is tall there, and on the tracks from levelling (diverting to the east).

Table 1. Overview on image acquisition, flight time in 2021 and weather conditions during the survey. Time zone UTC+2.

Imagery date	Time start	Time end	Peak solar elevation	Clouds	Wind
05 July	11.49	13.01	13.13	cloudy	gusty
03 August	13.51	15.03	13.15	variable	moderate
07 September	12.00	13.15	13.06	variable	variable

multispectral imagery of the study area in five spectral bands: blue (450 nm), green (560 nm), red (650 nm), red edge (730 nm) and NIR (840 nm). Each band has a spectral resolution of ± 16 nm except for NIR (± 26 nm). Additionally, an RGB camera in the same sensor system produces true colour images. After each flight, reflectance panel images were taken from a MAPIR Camera Reflectance Calibration Ground Target v2. These images were used for image calibration.

The flight altitude of 50 m resulted in a ground sampling distance of 2.76 cm. Flight speed was 3.5 m s^{-1} with a front and side overlap of 80 %. The overall duration for the 12,000 m flight route was about 70 min. The survey was conducted at ± 2 h around solar noon to minimise shadow effects; cloud and wind conditions varied (Table 1).

Image pre-processing relied on the workflow described by Hübner (2021), by which multispectral orthomosaics were created using pix4DMapper (https://www.pix4d.com/product/pix4dmapper-photogrammetry-software/). Although an RTK (real-time kinematic) base station was used for precise positioning, the orthomosaics had to be georeferenced individually using GCPs (ground control points, Figure 1c). The orthomosaics were masked by the study area and resampled to August geometry, so that all data could be stacked. The multispectral bands were used for the Typha classification and the NDVI.

In addition to the spectral data, a DSM (Figure 1d) for each month was processed using Structure from Motion in Agisoft Metashape Professional (v1.8) and the RGB and multispectral data. We compared the DSMs from the RGB and multispectral data. The multispectral DSM showed some artefacts we could not explain, therefore, we opted to use the RGB DSM which was otherwise similar. Using the height of the GCP in the south-eastern corner (Figure 1c), the DSM for each month was normalised to the local administrative elevation reference system (DHHN 2016). The DSMs were then resampled to the August spectral data and masked.

Reference information from the field were given as mean values per m². Therefore, we aggregated the DSM and NDVI data to a pixel size of 1 m (~1296 pixels m^{-2}). In doing so, the local variation in spectral or structural properties could be included in the modelling, e.g., via different percentiles (in addition to mean or maximum values), which helps in detecting canopy heterogeneity (Poley & McDermid 2020). Finally, we calculated different metrics from the DSM and NDVI during the process of aggregating to 1 m² resolution (i.e., p50, p60, p70, p80, p90, p100). The different metrics were separately tested in model performance for Typha biomass estimation.

DSM and NDVI values were extracted at the position of each training (in-situ harvests) and validation plot (Figure 1c). The centre coordinate of a plot was not always in the centre of the respective raster cell. Hence, we used a bilinear extraction method to get an interpolated value from the four nearest cells.

The analyses were undertaken in the R environment (R Core Team 2022, v4.2.2) using the packages terra (Hijmans 2022, v1.6-47), rgdal (Bivand *et al.* 2021) and randomForest (Liaw & Wiener 2002). QGIS (QGIS Development Team 2021, v3.22.14) was used for georeferencing, training, data collection, visualisation and map creation.

Field data collection

Data were gathered throughout the 2021 growing season, in the first week of July, August and September. During each week of fieldwork two different types of plots were sampled. Firstly, the 1 m^2 biomass plots with in-situ harvests of Typha, and secondly the 4 m^2 not-harvested, long-term plots. The destructive sampling (hereinafter 'training data') was used for model training, while the non-destructive sampling ('validation data') enabled the use of plots for validating model performance at multiple dates.

Training data

Typha biomass training data were harvested for each month of observation after the UAS surveys (32 plots in July, 12 each in August and September, Figure 1c). The area was categorised into three Typha density groups (low, medium and high density) and a fourth group representing Typha growing in *P. arundinacea* dominated stands. Three biomass plots per group and month were randomly distributed across the area using QGIS (v3.22.14). The minimum distance between training plots was 15 m, to spread the plots evenly across the entire area. A buffer of 3 m to validation plots was used to avoid overlap between training and validation plots. With this method, we were able to cover an even distribution of the plots along with the different main vegetation structures. In further analyses, grouping was discarded. A plot size of 1 m × 1 m was chosen due to heterogeneous Typha growth. The plots had to have at least one Typha shoot and should be in a homogenous patch of at least 3 m × 3 m. If Typha was absent, the vicinity was searched for a fitting plot.

The fraction cover of soil, water, moss, Typha and accompanying (non-Typha) vegetation was estimated in the field and the dominant species besides Typha

were identified. Further, the numbers of Typha shoots and inflorescences were counted. The standing height of ten ramets was measured with a folding ruler. All Typha biomass, such as leaves and flowers when present, was clipped at 3 cm above surface water level to ensure regenerative capacity (Sale & Wetzel 1983). It was assumed that the amount of Typha originating outside but growing into the plot was more or less equal to the amount of Typha originating within the plot but growing outside of it. Therefore, only plants originating within the plot were harvested. Biomass below surface water was neglected. The harvested plant parts were weighed in paper bags in the laboratory, dried for approximately 66 h at 70 °C, and weighed again. The weight of the paper bags was subtracted. Harvested biomass was used to model DAGB for the validation plots.

Validation data

The validation plots were examined simultaneously to the UAS surveys. From 80 long-term vegetation plots measuring 1 m × 4 m, 22 plots were randomly selected as validation plots and revisited every month (Figure 1c). The number of validation plots visited varied from 17 in June and 12 in August to 8 plots in September, due to time constraints. A few plots were sampled only once throughout the whole vegetation period. Plot orientation was south–north and each validation plot was divided into four 1 m × 1 m subplots. At each subplot, the same metrics as for the training plots, apart from Typha harvests, were recorded. Further, field data were supported by comprehensive photo documentation. To achieve consistency between image and reference data, the training and validation plots were positioned according to plot markers visible in the orthomosaics in QGIS.

Biomass for the validation plots was predicted non-destructively. Thus the validation plots, which were spatially independent from the training data, could be reused throughout the vegetation period. The model to predict biomass for these validation plots was based on the in-situ harvests from the training plots using linear regressions (Figure 2). The harvested biomass data were pooled for the field model because the observation dates had no influence on biomass. This way, the data set was increased to 56 plots in total.

We tested several independent variables (mean height, number of shoots, mean height + number of shoots, mean height + number of flowering shoots, number of shoots + number of flowering shoots). Different transformations of DAGB as dependent variable (natural logarithm, square root and no transformation) were also tested. The y-intercept was set to 0, expecting no biomass for zero shoots, flowers, and/or height for the validation plots.

The final model (Table 2) was chosen using $R^2_{adj.}$, and leave-one-out cross-validation (LOOCV) with MAPE (mean average prediction error) and RMSPE

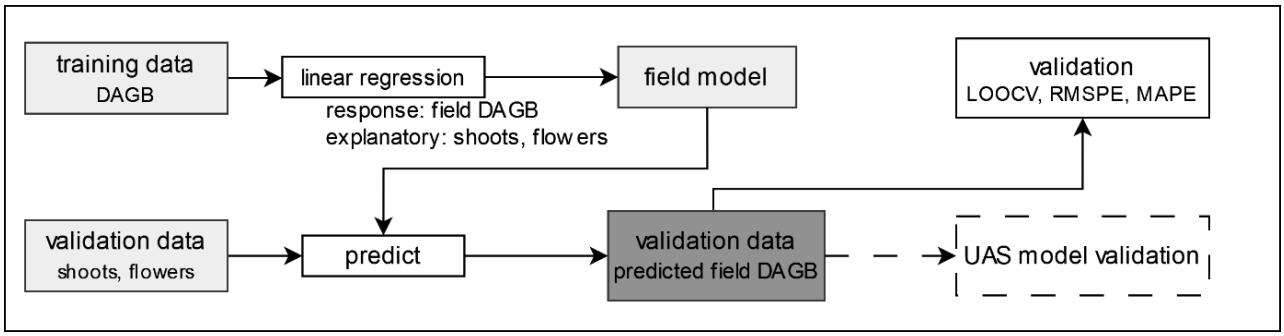

Figure 2. Workflow for non-destructive biomass prediction for the validation plots. Different response variables (transformations of field DAGB) and explanatory variables were tested. In dark grey the final product (predicted field DAGB) that will be used for final UAS model validation (dashed lines). DAGB = dry aboveground biomass, LOOCV = leave-one-out cross-validation, MAPE = mean absolute prediction error, RMSPE = root mean squared prediction error.

Table 2. Regression equation for the final field model based on flowers and shoots. DAGB = dry aboveground biomass, MAPE = mean absolute prediction error, RMSPE = root mean squared prediction error. MAPE and RSMPE based on leave-one-out cross-validation. fl = no. flowers, sh = no. shoots.

Regression equation	$R^2_{adj.}$	p-value	MAPE (g m^{-2})	RMSPE (g m^{-2})
DAGB = 33.08fl + 4.79sh	0.90	< 0.01	56.0	81.6

(root mean squared prediction error) (Figure 2). Non-destructive biomass prediction was used to validate UAS biomass.

Data analysis

Typha classification

In the literature it is recommended to combine spectral metrics, e.g., NDVI (or other VIs), and height metrics (Luo *et al.* 2017, Poley & McDermid 2020, Lu *et al.* 2022). However, for mixed vegetation stands, a non-stratified approach based on NDVI and height metrics will achieve a similar range of biomass for all species and not just the target species. Thus, we created a Typha classification from multispectral data (blue, green, red, red edge, NIR). The Typha classification was then used to estimate the share of Typha per 1 m² pixel and thus disentangle the fraction of Typha and non-Typha biomass. The resulting Typha fraction cover mask (FC) was in the end used to mask the final biomass model and was applied to the raster. The masked biomass map was compared to the respective unmasked biomass map.

Typha was mapped at the original resolution of the multispectral data (2.76 cm) and tested for three different input data sets, i.e., August only (5 bands), average reflectance for the three months of observation (5 bands) and a stack of all months (15 bands) (Figure 3). The resulting Typha classifications were named according to their input data (cl_{Aug}, cl_{mean}, cl_{stack}). The study area was classified into three classes: Typha, non-Typha, and water. 225 points were sampled using QGIS (v3.22.14) as training data, comprising 130 non-Typha, 71 Typha and 24 water points. We used the randomForest package (Liaw & Wiener 2002) based on Breiman (2001), with *ntree* = 500 (Beyer *et al.* 2019). The three resulting classifications were spatially filtered: isolated pixels of a given class that were surrounded only by pixels of a different class were assigned to the different class.

The best classification was chosen based on the out of bag (OOB) error, accuracy assessment with independent validation points, and expert knowledge during visual assessment of class distributions. For the accuracy assessment and final confusion matrix, 50 points per class (150 in total) were randomly sampled as validation points from the cl_{mean}, to which the actual classes were assigned. For the FC, the final best classification was aggregated to one metre while calculating the share of Typha pixels m^{-2} (Figure 3). We used a min-max normalisation for the final, normalised Typha fraction cover mask (FC_{norm}). The thresholds for the minimum and maximum values were tested iteratively and adjusted according to Typha density cover in different regions using knowledge of the study site. Typha with a fraction cover of < 3 % and thus only 300 cm^2 was most likely to be Typha overestimation. Therefore, the final threshold for the minimum values was set to 3 % (< 3 % fraction cover = non-Typha). A density of 59 % was already representative for dominant Typha stands because their erect growth form results in comparably large cover fractions of shadow. At such densities, no relevant biomass from other plant species was observed. Thus, all values > 59 % were set to 100 %, to keep high Typha densities and thus high Typha biomass.

Model fitting and validation

We tested different models to predict standing biomass above the water level from DSM and NDVI

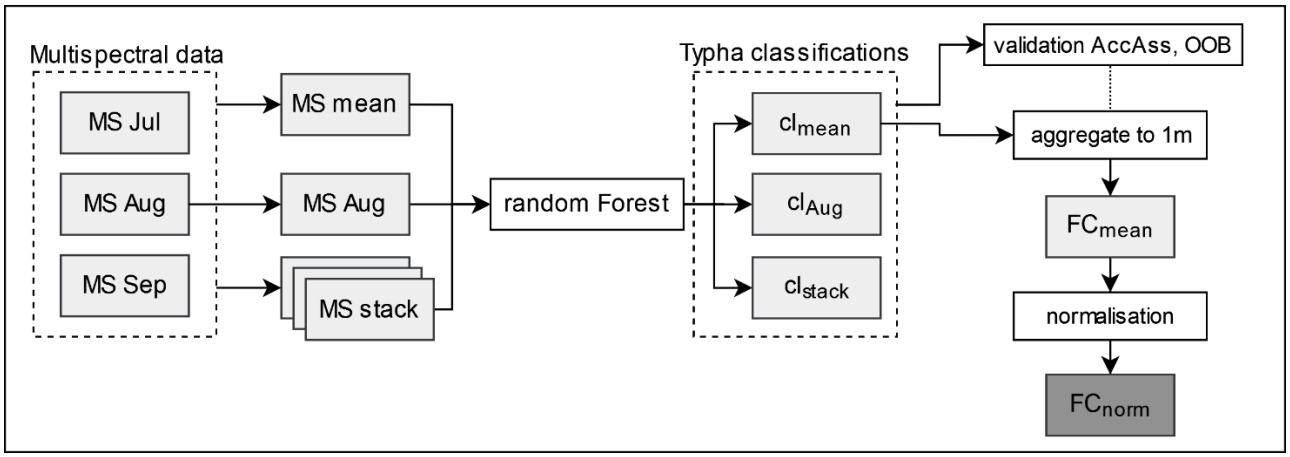

Figure 3. Workflow for Typha fraction cover (FC) mask. Final product (FC_{norm}) in dark grey. The dotted line represents the influence of the validation on the classification to be aggregated (MS = multispectral, cl = classification, AccAss = accuracy assessment, OOB = out of bag error, norm = normalised).

UAS metrics (Figure 4). We built simple linear regression models for August with different transformations of biomass (natural logarithm, square root and no transformation) since simple linear regression models are commonly used for biomass prediction (Doughty & Cavanaugh 2019, Cunliffe *et al.* 2020, Räsänen *et al.* 2020, Doughty *et al.* 2021, Räsänen *et al.* 2021, Cunliffe *et al.* 2022). Regarding vegetation height, Cunliffe *et al.* (2022) proposed to set the y intercept to zero, reflecting no biomass for zero height. We deviated from this approach because our target was a model which is effective within our data range. Nevertheless, this may result in negative biomass prediction. To take non-linear trends into account, we further tested a power regression equation and a 3rd degree polynomial model. The models were derived separately for each DSM and NDVI metric (p50, p60, p70, p80, p90, p100) as predictor variable and DAGB as the response variable and afterwards applied to the respective DSM or NDVI raster. The resulting maps were then multiplied with the FC_{norm} (Figure 4).

For validation, biomass predictions from UAS data were compared to biomass modelled from field data for the validation plots (Figure 2, Figure 4). For these data pairs, RMSE (root mean squared error) and MAE (mean average error) were calculated. Scatterplots were evaluated visually and by fitting a linear regression and 1:1 line. The model with a regression function closer to the 1:1 line is considered better, when RMSE and MAE are comparable between the investigated models, since the errors from over- and underestimation tend to balance out.

To test the temporal transferability of the approach, the best model from August was applied to the respective July and September DSM metrics and validated with the non-destructive biomass prediction from field data for the respective months. Biomass development was evaluated by calculating the DAGB differences between August and July prediction rasters and between September and August prediction rasters.

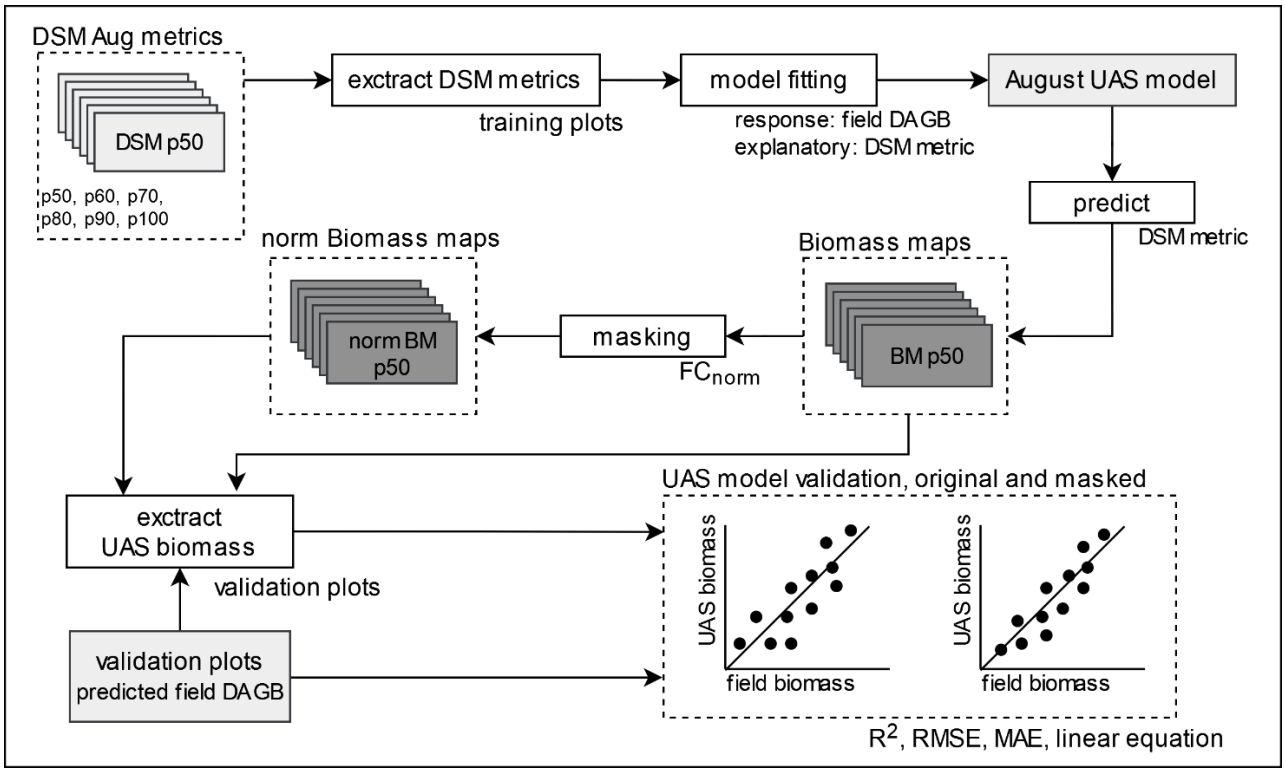

Figure 4. Workflow for the biomass prediction maps, exemplary for DSM. For the NDVI models, DSM metrics were exchanged with NDVI metrics. Model fitting and model predictions are applied to each DSM percentile separately. Model fitting and prediction were repeated for each model type (simple linear regression, power regression equation and 3rd degree polynomial model) and the different transformations of DAGB (DSM = digital surface model, BM = Biomass maps, FC_{norm} = normalised Typha fraction cover mask, DAGB = dry aboveground biomass). Final products in dark grey. (Please note: The workflow for the FC_{norm} was described in Figure 3 and for the non-destructive biomass prediction for the validation plots in Figure 2.)

RESULTS

Typha classification

The classification of Typha, non-Typha and Water resembled the situation on the ground. Typha appeared at different densities with the highest densities towards the very west of the area. Water was visible, especially in the south-east, where elevation was lowest. Non-Typha vegetation appeared both in patches and intermixed with Typha and included, e.g., *Juncus* spp. in the east, *Carex* spp. close to the open water in the south-east, *P. arundinacea* in the south-west and *P. australis* at the north-western edge (Figure 5). However, Typha was overestimated for small patches of plant shadows.

Validation showed the best result for cl_{mean} with an overall accuracy (OA) of 80 % (OOB error = 16.44 %) compared to cl_{aug} (OOB error = 13.78 %, OA = 75 %) and cl_{stack} (OOB error = 9.33 %, OA = 73.3 %). Further, the errors of omission (26.7 %) and commission (34 %) for Typha were more balanced for cl_{mean} and the error of omission was the lowest overall. The F1 scores were generally highest for cl_{mean} and the three classes Typha, non-Typha and Water (0.7, 0.72 and 0.99, respectively). The F1 for cl_{aug} was higher (0.75) only for non-Typha.

Mapping August biomass

Overall, model fitting of the linear regression and the August DSM training data was best for the p50 DSM (R^2_{p50} = 0.83), although the difference to the other percentiles was rather small (e.g., R^2_{p90} = 0.81). The NDVI training data on the other hand explained 35–62 % of the variation in the data (R^2 = 0.35–0.62), with increasing performance for higher percentiles. For p100 DSM (R^2_{p100} = 0.54), outliers - particularly for greater DSM heights yet lower DAGB values - had a negative influence on the model regression quality (R^2) for all model types, which was similar to p100 NDVI. Thus, p100 was discarded in further analyses, and figures from here were restricted to p50, p70, and p90. For NDVI, p80 was used instead of p70 because p80 NDVI performed better (R^2_{p70} = 0.48, R^2_{p80} = 0.55).

The Typha biomass maps for August followed the biomass patterns on the ground. Generally, high biomass was found in the north-western parts and low biomass in the eastern parts (1a and 5a in Figure 6). Further, the former ditch stretching from north to south was overgrown by tall Typha plants and, thus, high biomass. Typha biomass was overestimated where non-Typha species were found. Applying the Typha fraction cover mask (FC_{norm}) to the biomass prediction improved the predicted biomass for non-Typha areas. For the DSM, predicted intermediate biomass improved to low biomass in large areas, especially west of the ditch stretching from north to south and in the south-western region (1b in Figure 6). The NDVI predictions improved especially in a large area in the centre of the study area (5b in Figure 6).

Validation – August biomass

In general, model performance was best for the p90 DSM and p80 NDVI and, in both, biomass prediction was improved by using the min-max normalised Typha mask (FC_{norm}). Performance of the DSM models increased with increasing DSM percentiles, and was best for a simple linear regression and p90 DSM (y = -558 + 5.6x, $RMSE_{p90}$: 136 g m^{-2}, MAE_{p90}: 109 g m^{-2}). The FC_{norm} performed best with the p90 DSM reducing prediction errors ($RMSE_{p90masked}$: 115 g m^{-2}, $MAE_{p90masked}$: 86 g m^{-2}) (Figure 7). Further, the regression lines got closer to the 1:1 line, compared

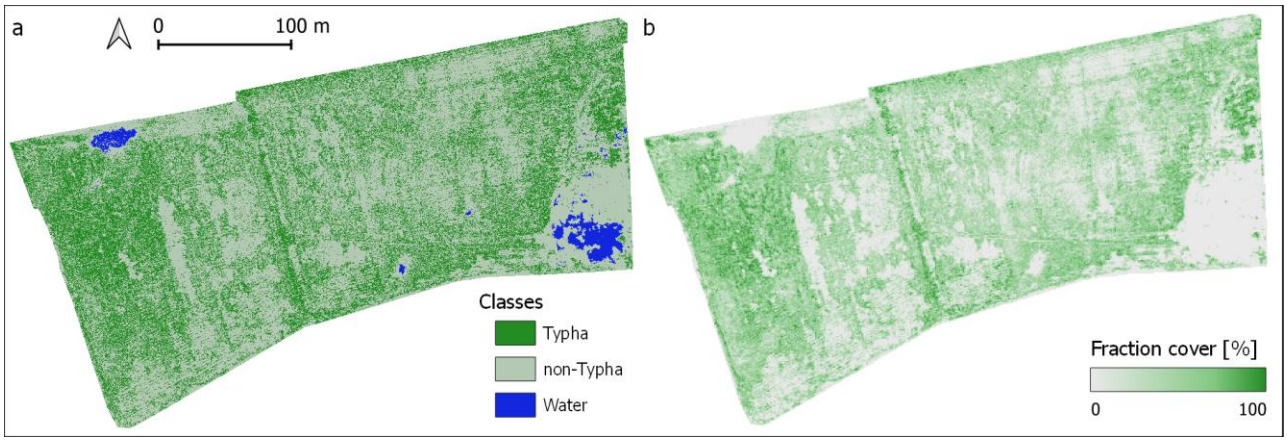

Figure 5. a) Original Typha classification, based on the average reflectance of the months July to September across the bands (cl_{mean}). b) Normalised fraction cover mask of Typha (FC_{norm}), with thresholds from 3 % (< 3 % = no Typha) and 59 % (> 59 % = 100 %).

to the respective original biomass. Especially the overestimation of low biomass improved with the FC_{norm}. However, similar trends to the original predictions were observed such as the overestimation of high biomass and the underestimation of intermediate biomass, although the slope of 1 indicates that the error was more balanced out in both directions.

In comparison, the p80 NDVI model (y = -2973 + 4116.2x, $RMSE_{p80}$: 109 g m^{-2}, MAE_{p80}: 88 g m^{-2}) performed best among all NDVI models and was improved by the FC_{norm} ($RMSE_{p80masked}$: 103 g m^{-2}, $MAE_{p80masked}$: 74 g m^{-2}) (Figure 7). Overestimation of low biomass improved with the mask, although the trend remained. The regression line with a slope < 1 indicated an underestimation of high biomass, which was opposed to the DSM models. Further, biomass saturated at approximately 500 g m^{-2}. We therefore show the multitemporal transferability only for the p90 DSM model.

Multitemporal application

Harvested Typha biomass varied over time and ranged from a minimum of 2 g m^{-2} in June to a maximum of 741 g m^{-2} in August (Table 3, Field DAGB). The predicted UAS biomass for the training plots, on the other hand, were generally lower and ranged from -153 g m^{-2} original and -114 g m^{-2} masked, to a maximum of 526 g m^{-2} for both.

For July and September, the areas of high and low biomass matched the August prediction (Figure 8) when the linear p90 DSM August model was applied

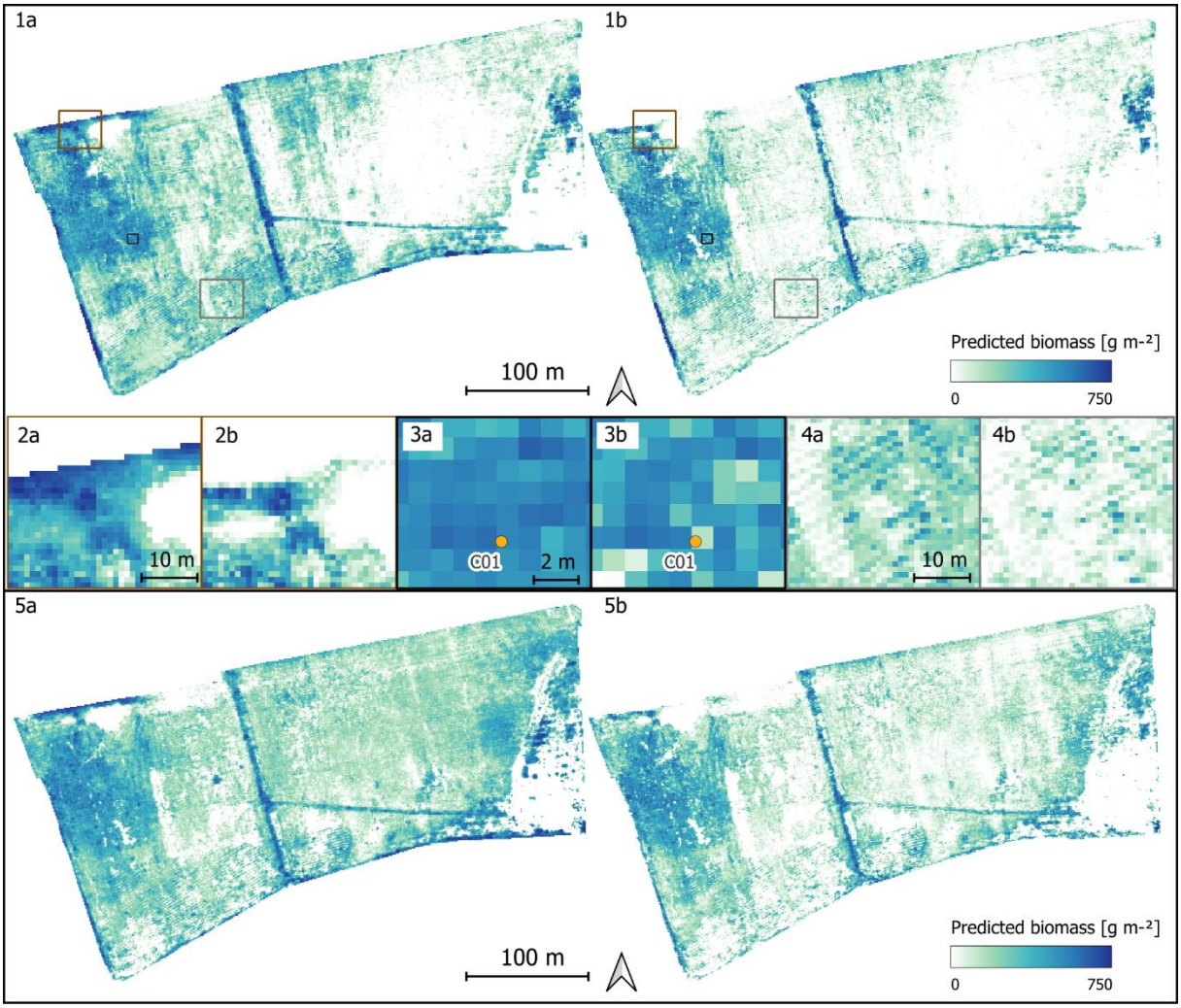

Figure 6. 1: Comparison between the original biomass prediction (always a) for August with the p90 DSM linear regression model (y = -558 + 5.6x) and the masked biomass prediction (always b). Highlighted areas (2–4 from west to east) show the influence of the Typha mask on the original biomass prediction. 2: Exclusion of *Phragmites australis* as a non-target species. 3: Masking resulted in Typha biomass underestimation. 4: Exclusion of *Phalaris arundinacea* as a non-target species. 5: Comparison between the original (a) p80 NDVI linear regression model (y = -2973 + 4116.2x) and b) the respective masked biomass prediction (DSM = digital surface model, NDVI = normalized difference vegetation index).

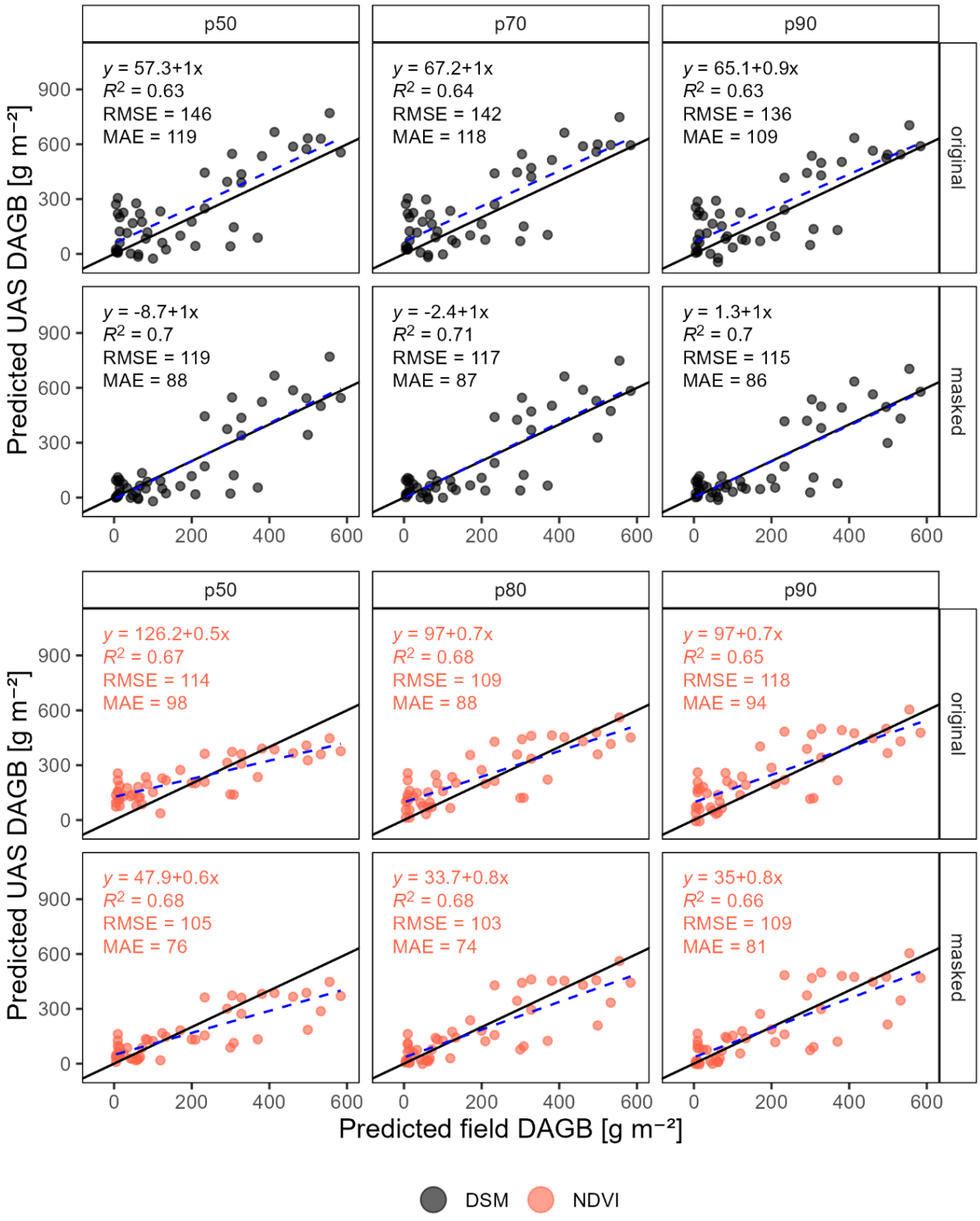

Figure 7. Validation plots for different August DSM and NDVI metrics (p50, p70, p90) and a linear regression, with and without masking. Please note that for NDVI the p80 metric is shown. Predicted field biomass based on shoots and flowers from pooled July, August and September data (DSM = digital surface model, NDVI = normalized difference vegetation index, DAGB = dry aboveground biomass, 1:1 line in black, fitted regression line in blue). n = 46.

Table 3. Field ground-truth data (min = minimum, mean, and max = maximum) of the training plots for July, August and September and their respective UAS original and masked biomass predicted from the final p90 DSM model (DAGB = dry aboveground biomass).

	Min DAGB (g m^{-2})			Mean DAGB (g m^{-2})			Max DAGB (g m^{-2})		
	Jul	Aug	Sep	Jul	Aug	Sep	Jul	Aug	Sep
Field	2	7	19	143	200	176	725	741	347
UAS original	-153	-63	-130	107	200	111	526	515	283
UAS masked	-114	-21	-64	78	145	82	526	515	250

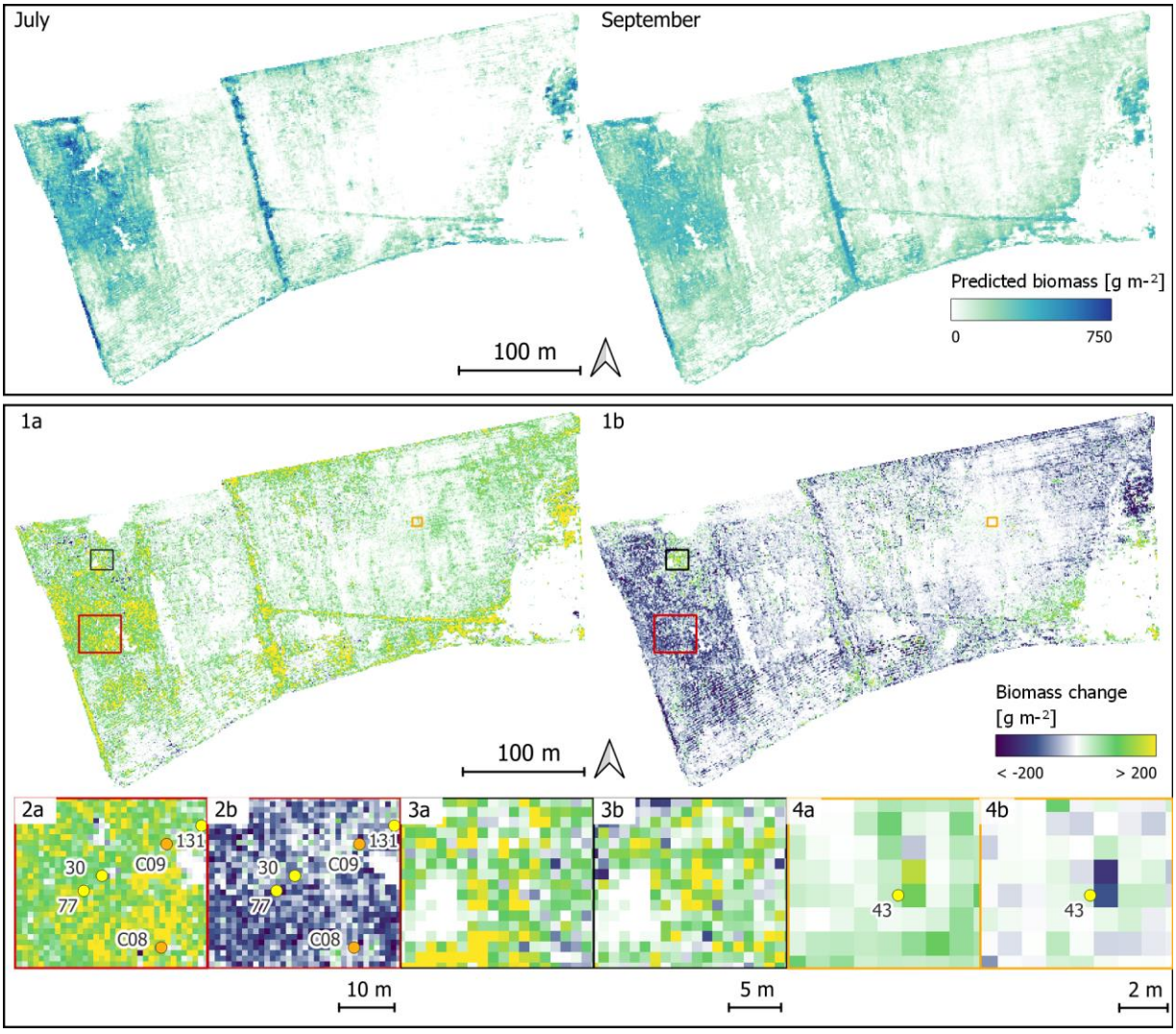

Figure 8. Top: Biomass maps for July (left) and September (right) predicted from the p90 DSM August model (y = -558 + 5.6x) with Typha mask. Bottom: Comparison of biomass development from July to August (always a) and August to September (always b) for (1) the whole study area. Highlighted areas (2–4 from west to east) show different changes in biomass. 2: Increase in biomass from July to August (a) in a dense Typha stand with high Typha biomass but a decrease from August to September (b). 3: Increase in biomass at an open water body for both, from July to August and August to September. 4: Increase in biomass from July to August (a) and a decrease in Typha biomass resulting from harvested Typha in August (DSM = digital surface model).

to July and September. The development from July to August indicated an increase in biomass especially for the areas in which Typha was dominant (2a in Figure 8), but a decrease in biomass for almost the same areas from August to September (2b in Figure 8). An increase in biomass was observed for the ditch stretching from north to south (1a and 1b in Figure 8) and close to open water bodies (3a and 3b in Figure 8). Typha biomass harvested in August was visible in the September prediction (4a and 4b in Figure 8).

Validation - multitemporal application

The validation of July p90 DSM data resulted in RMSE and MAE values comparable to August, for both, with and without masking ($RMSE_{p90\_Jul}$: 135 g m^{-2} and MAE_{p90_Jul}: 99 g m^{-2}, $RMSE_{p90masked\_Jul}$: 119 g m^{-2}, $MAE_{p90masked\_Jul}$: 84 g m^{-2}). In July, the slope of the linear regression was low (0.6; Figure 9) while having a comparably high y-intercept (original: 59.2, masked: 33.7), indicating overestimation of low biomass and underestimation of high biomass. Model performance for September was slightly better ($RMSE_{p90\_Sep}$: 124 g m^{-2}, MAE_{p90_Sep}: 98 g m^{-2}, Figure 9). An improvement was again visible for the masked biomass prediction in the mean average error ($MAE_{p90masked\_Sep}$: 92 g m^{-2}) because the overprediction of low biomass was reduced.

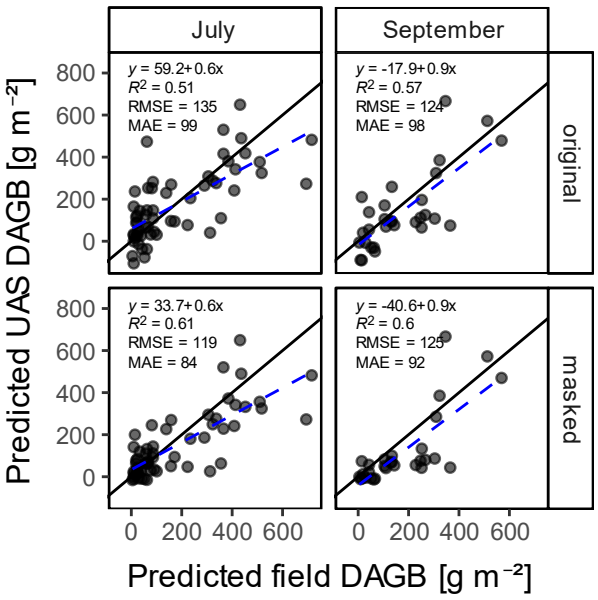

Figure 9. Validation plots for July and September, with the p90 DSM August model (y = -558 + 5.6x), original and masked (DSM = digital surface model, DAGB = dry aboveground biomass, 1:1 line in black, fitted regression line in blue). For July n = 58, for September n = 30.

DISCUSSION

Predicting Typha biomass for August

Our Typha classification and biomass prediction maps matched the heterogeneous growth patterns and spatial distribution of Typha, as observed and measured (2–741 g m^{-2}) during fieldwork, well. The maximum values of harvested and predicted biomass were mainly observed in the western parts, where Typha was dense and dominant (high fraction cover and tall Typha plants). Low Typha biomass was predicted for the eastern parts, where fraction cover and height were accordingly low. Non-Typha was dominant in these parts (i.e., *Juncus* spp.). The comparably low total biomass of 1.16 t ha^{-1} (2–20 t ha^{-1} after rewetting shown in Timmermann 2003, Heinz 2011, Schulz *et al.* 2011, Geurts *et al.* 2020) predicted from the masked August model is supported by unfavourable growing conditions. Delayed planting in 2019, herbivory and high water level fluctuations in 2020 resulted in low Typha development. For some parts in the western area, on the other hand, where water tables were generally higher, biomass yields of approx. 5–6 t ha^{-1} could be reached.

Various studies have shown that comparisons between field measurements and heights derived from lidar or SfM can have a positive (Madec *et al.* 2017, Cunliffe *et al.* 2020) or negative (Wang *et al.* 2009) bias. Thus, we tested a linear regression between the extracted DSM heights for the plots and the respective in-situ Typha measurements, which proved significant ($R^2 = 0.64$, $p < 0.05$ for August). In our case, a slope < 1 indicates a negative bias, thus underestimation of tall plants. Nevertheless, since the negative bias is identical for model training and model application, DSM heights can be used for mapping and in the end the DSM constitutes a proxy for vegetation height in biomass prediction.

The usability of the DSM is further supported by our analysis. The DSM metrics showed a significant ($p < 0.05$) linear relationship ($R^2 = 0.54–0.83$ for August) to biomass training data. The NDVI metrics were significant as well ($p < 0.05$), but with less explanatory capacity ($p < 0.05$, $R^2 = 0.35–0.62$). Further, the linear regression without transformation proved the most stable compared to the power regression model and the square root transformation (comparisons not shown). This confirms the findings of Cunliffe *et al.* (2020), who were able to find a linear relationship between harvested biomass for shrub vegetation and UAS derived height ($R^2 = 0.90$) in a tundra landscape. Mean canopy height proved to predict biomass at species level well throughout different non-forest ecosystems (Cunliffe *et al.*

2022). Aggregating the height distribution into metrics, which served as model input, proved helpful to account for canopy structure. DSM metrics outperform NDVI metrics where vegetation height was low but NDVI values were high, which applied to *Juncus* spp. in the eastern area. With DSM percentiles starting from 50 % (p50), smaller fractions of low vegetation height within the aggregated 1 m^2 plots were neglected. NDVI values of vital but small plants on the other hand are still high resulting in high biomass values.

Higher DSM percentiles showed improved model performance: with p90, the Typha heights of plants that were higher than the accompanying vegetation of the same plot were considered better even when they did not constitute the majority of the area. At the same time, individual outliers were neglected. Further, high biomass was less overestimated by the p90 than by the p50 model, reducing RMSE and MAE. These findings confirm Luo *et al.* (2017), where high percentiles of lidar point clouds resulted in the highest accuracies in estimating *P. australis* biomass ($R^2 = 0.58$). Furthermore, Poley & McDermid (2020) stated that metrics, apart from mean and maximum variables, are better suited to describe heterogeneous canopy and thus biomass, depending on target species. This can be further supported by our study, where the p100 DSM metric resulted in low model performance due to less stability with regard to outliers. Intermediate biomass levels were underestimated in our DSM maps, e.g., east of the ditch (see 1a in Figure 6), where the NDVI maps were more reliable (see 5a in Figure 6). In these parts, vegetation height was comparatively low while shoot and flower count were intermediate, resulting in low DSM biomass. Typha stands of low height and intermediate shoot count showed NDVI values that were better correlated to biomass.

Structural and spectral information could not account for flower weight. The UAS models relied on height or greenness, but the fieldwork showed that the number of flowers had a positive influence on absolute biomass while not being related to either plant height or greenness. Therefore, the observed underrepresentation of intermediate Typha biomass occurred where Typha height and shoot count were intermediate but flower count was relatively high. The predicted field biomass for validation, on the other hand, was based on shoots and flowers and thus took into account the higher biomass resulting from flowers. This limitation appeared in the validation scatterplots (Figure 7, 300–400 g m^{-2} field biomass compared to 25–110 g m^{-2} DSM and NDVI biomass). The effect of flowers might be smaller for developed Typha stands where plants are taller and, hence, the contribution of flowers to the total biomass is smaller. Flights at lower altitudes would give a higher resolution for the RGB orthophoto. Object detection using AI could be tested (Zaidi *et al.* 2022) to get, for example, a flower count per area. Nevertheless, our aim was to test the combination of different data sets that could be derived from an affordable single UAS survey at reasonable altitude per observation date.

When flower and shoot counts were intermediate but Typha very tall, on the other hand, high biomass was overestimated by the DSM model (field prediction: 400–550 g m^{-2}, UAS prediction: 550–700 g m^{-2}, Figure 7). The offset of high DSM biomass compared to biomass modelled from field data might result from the field prediction model itself - after extensive testing, only shoots and flowers were used as explanatory variables, as they proved most accurate statistically (lowest MAPE and RMSPE in LOOCV). To better account for high biomass resulting from tall plants, plant height would be needed as input variable for these ranges.

Improving predictions with Typha mask

The biomass distribution across the study area was better represented by the masked biomass than for the original biomass map. Large areas of non-Typha vegetation as well as overestimations in areas of mixed vegetation composition could be excluded successfully, for DSM and NDVI models, resulting in smaller errors and a more even distribution of over- and underestimation.

The Typha fraction cover mask (FC_{norm}) from the 5-band multispectral sensor detected non-Typha species reliably for large areas and was able to improve the prediction, where strong biomass overestimation resulted from the presence of non-target species (DSM $RMSE_{p90}$ = 136 g m^{-2}, $RMSE_{p90masked}$ = 115 g m^{-2} and MAE_{p90} = 109 g m^{-2}, $MAE_{p90masked}$ = 86 g m^{-2}, Figure 7). This also applied to NDVI, although less pronounced (NDVI $RMSE_{p80}$ = 109 g m^{-2} to $RMSE_{p80masked}$ = 103 g m^{-2}). Overestimation of Typha biomass could be reduced where species such as *Carex* spp. or *P. arundinacea* reached similar heights to Typha. Especially *P. arundinacea* was dominant west of the ditch stretching from north to south and in the south-western region. In these parts with heterogenous vegetation, Typha fraction coverage and, hence, the values of the FC_{norm}, were relatively low and consequently the biomass prediction reliably improved (4a and 4b in Figure 6). Further, *P. australis*, as a tall growing plant, could be excluded successfully with the FC_{norm} (2a and 2b in Figure 6). For the NDVI model, *P. arundinacea* was already excluded in the original maps, because

advanced senescence of the species resulted in lower NDVI values, and thus low biomass, compared to healthy Typha stands. Nevertheless, the FC_{norm} improved the prediction for a large area in the middle of the study site where *Juncus* spp. were dominant.

However, errors of the fraction cover map might be propagated to the final biomass map. The F1 scores for Typha and non-Typha of 0.7 and 0.72, respectively, indicate some confusion between the two classes. The shadow of *P. australis* was misclassified as Typha, visible as the elongated patch at the south-western edge (Figure 6). The min-max normalisation, on the other hand, improved the errors of the fraction cover mask in dense Typha stands. In the western parts where Typha was dominant, shadow coverage was high due to the erect growth of Typha. As a result, cover fraction values of 100 % could not be reached. With a maximum value of 59 % for the min-max normalisation, we ensured to keep these areas as pure Typha stands with high biomass predictions. Only small areas were negatively affected by the mask in high density areas because of high shadow fractions (3a and 3b in Figure 6). As the positive effects clearly outweigh the negative ones, and RMSE and MAE were improved, the idea of incorporating a species mask from the same UAS proved successful.

The usage of a species-specific mask in combination with a DSM is advantageous over the NDVI. All NDVI models showed a strong saturation effect at a biomass value of 500 g m^{-2}, which was to be expected from literature (Tucker 1977, Cunliffe *et al.* 2020). Thus, a biomass increase or high biomass in general might be hard to detect, especially for dense Typha stands. Non-target species with similar NDVI signatures to Typha could be excluded with the FC_{norm}. The DSM model performance was also slightly weaker for high biomass (maximum values Table 3, NDVI not shown), especially when plants were tall and fraction cover and flower count high. But the validation scatterplots and prediction maps showed no saturation effect as such (slope = 1), which is preferable.

To overcome these saturation effects, we further tested a combination of all ten DSM and NDVI metrics (p50–p90) with a machine learning algorithm (Random Forest). Although the validation results were promising, with an R^2 of 0.69 for the masked model and comparably good RMSE and MAE values (107 g m^{-2} and 79 g m^{-2}, respectively), the validation scatterplots indicated a strong over- and underestimation of intermediate biomass (results not shown).

To conclude, a model based on DSM metrics proved helpful in dense stands with tall Typha plants. This will become even more relevant in the paludiculture context, where high biomass production of tall paludiculture crops is targeted and management effects shall be monitored for such stands. NDVI based models would saturate on such stands and, therefore, DSM based models should be considered. The mask showed good accuracies for our study area, where Typha distribution is heterogenous and intermixed with non-target species, and is recommended for future applications. The denser Typha stands in subsequent years can be expected to lead to even higher classification accuracies.

Model transfer to July and September

Harvested biomass of the training plots and measured height and shoot development for all plots indicated a biomass accumulation over time (Figure 10). Maximum biomass harvested in September was comparably low (Table 3), because the plots were situated in sparser parts of the dense Typha area in the west. Nevertheless, biomass increase was observed from August to September (Figure 10). The relative number of flowers remained the same throughout the months.

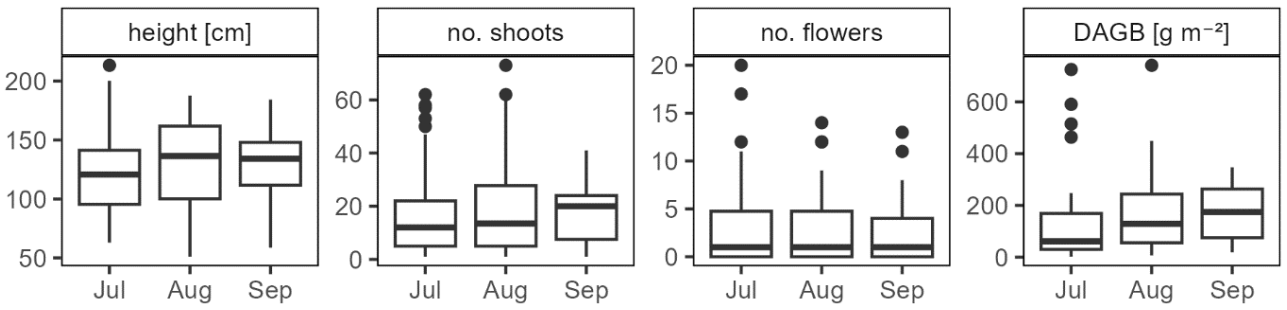

Figure 10. Development of height, number of shoots and number of flowers from July to September for the training and validation plots combined. Dry aboveground biomass (DAGB) development from July to September for the training plots only.

An increase in biomass from July to August was observed for the DSM biomass (Figure 8). High biomass and low biomass areas generally coincided with August biomass distribution. High changes in biomass were mainly observed for areas in which Typha became denser or taller. Changes of +200 g m^{-2} from July to August resulted from a change in DSM height of roughly +30 cm. In areas where Typha density and biomass were low, small or no changes in biomass were found, which coincides with the evidence from the field. New shoots developing during the vegetation period (Figure 10) were mainly found in close vicinity to older Typha shoots. It can be concluded from this that rhizomatous growth was the main driver for the spreading of Typha in the study area in 2021.

The development of UAS biomass from August to September, on the other hand, showed a drop in biomass, which was opposed to field biomass and the evidence from fieldwork (Figure 10). In our prediction, an increase in biomass from August to September occurred only on areas where open water was overgrown by Typha (north-western and south-eastern areas, 3a and 3b in Figure 8). The dominating decrease in biomass resulted from the DSM development over time. The DSM indicated a decrease in height from August to September, which cannot be confirmed by the field data (Figure 10). These discrepancies might arise from the differences in what the height represents - the field height represents the mean of ten random Typha shoots per plot, while the DSM height represents the (respective percentile) height of all vegetation parts. As the Typha leaves have a tendency to bend with increasing senescence, this might result in lower DSM metrics and, consequently, lower biomass predictions. Moreover, the underestimation of September biomass may be reduced by lower quality of the DSM, which may have suffered from more shadow fractions due to lower sun elevation as well as decreased contrast due to starting senescence. However, the experimental setup in the field does not allow investigation of this matter and, further, quite labour-intensive experiments would be required. Still, the general applicability and model performance proved appropriate for the in-situ training plots for August, where harvests were clearly detected in the September map as true biomass decrease.

The height-based model proved more stable with regard to model transferability. Transfer of the p80 NDVI still resulted in a clear underestimation of high biomass for both months. The transfer to July was even more problematic than to September, because NDVI values were comparably low for reasons we do not understand and, thus, predicted biomass was low for all validation plots (RMSE = 339 g m^{-2}, MAE = 265 g m^{-2}).

To conclude, the multitemporal applicability of the height-based model relies on observable development of plant growth. This further supports the assumptions that model performance is dependent on the growth stage (Poley & McDermid 2020) and that more training data are needed.

Methodological considerations

Despite the presented strength of the approach and the clear positive effect of using DSM metrics and a species mask, several limitations need to be considered. The surface of the study area was flat, since it was levelled before rewetting. If regional elevation differences exist, normalisation of the underlying DSM using a digital terrain model could be considered. Further, the DSM was generated from RGB data only, using structure from motion, which can be a challenging approach for reconstructing the real top of vegetation (Madec *et al.* 2017). Lidar data might yield more variance for tall plants and thus would be interesting to test for improved model performance. We neglected the biomass below the water level, which in terms of paludiculture is separate from the yield. With regard to root biomass as an indicator for carbon accumulation (Schwieger *et al.* 2021), it would be further interesting to estimate below ground Typha biomass. Lopatin *et al.* (2019), for example, already showed an improvement in below ground carbon stock estimation in a Chilean peatland from combining plot-based field information with UAS proxies.

A plot size of 1 m × 1 m was chosen, due to heterogeneous Typha growth, although smaller plot sizes of 0.25 m × 0.25 m are mentioned in the literature (Doughty & Cavanaugh 2019, Räsänen *et al.* 2019, Cunliffe *et al.* 2020, Doughty *et al.* 2021, Räsänen *et al.* 2021, Cunliffe *et al.* 2022). As a result, when plot area and raster cells had a small mismatch, larger areas (two or more raster cells) might be affected by, e.g., biomass change. In future research, when addressing heterogenous vegetation structures, it is recommended to sample plots of smaller sizes than 1 m^2 because, with UAS data, small scale differences can be captured well. Moreover, reduced plot size could increase sample size while keeping the labour requirement similar.

CONCLUSION

UAS data has great potential in bridging the gap between small and larger scale landscape analyses (Doughty *et al.* 2021, Lu *et al.* 2022); with satellite imagery, large areas can be covered but spatial resolution is low, while UAS imagery covers small areas yet offers high spatial resolution. From one single drone survey using an affordable UAS, different data sets can be derived: structural data (DSM) from the RGB as a proxy for vegetation height, and multispectral data for species-specific stratification. Biomass prediction from a DSM showed good accuracies when biomass increase correlated with an increase in height. DSM-based models could account better for high biomass than NDVI-based models. The combination of structural and spectral data, e.g., with a species mask, is especially recommended when the distribution of the target species is heterogeneous and it is intermixed with non-target species. A species mask outperforms results from vegetation indices alone, where different species show similar spectral signatures. Problems can arise from changes in overall plant appearance such as fructification, where comparably heavy plant parts cannot be detected from height or spectral signatures. This affects model transfer over time. Our approach worked well for one paludiculture target species, *T. latifolia*, and can be assumed to be directly transferable to many others, as its emergent macrophyte growth form is shared with other potential paludiculture crops such as *P. australis*, *P. arundinacea*, *Carex* spp. and many others. It could be promising to test the workflow for these species; this research could yield valuable insights for optimising the contributions of paludiculture to global efforts in climate change mitigation.

ACKNOWLEDGEMENTS

This research was carried out in the scope of the PRIMA project, which was funded by the Agency for Renewable Resources (Fachagentur Nachwachsende Rohstoffe e.V., FNR), Germany, on behalf of and with funds from the Federal Ministry of Food and Agriculture (Bundesministerium für Ernährung und Landwirtschaft, BMEL), Germany [FKZ 22026017]. The authors thank several student collaborators, especially Carla Prüfer, for assistance during fieldwork. This work was inspired by the ideas and the master thesis of our friend and colleague Fabian Hübner (1993–2023) who died while this manuscript was being written and to whom it is dedicated.

AUTHOR CONTRIBUTIONS

CH: conceptualization, methodology, formal analysis, investigation, writing (original draft), visualization; BB: investigation; FH: investigation; NK: investigation; JK: conceptualization, resources; SvdL: conceptualization, methodology, resources, supervision; all authors: writing (review and editing).

REFERENCES

Abel, S., Couwenberg, J., Dahms, T., Joosten, H. (2013) The database of potential paludiculture plants (DPPP) and results for Western Pomerania. *Plant Diversity and Evolution*, 130, 219–228.

Beyer, F., Steiger, A., Grenzdörffer, G. (2019) Multitemporale Auswertung von Moor-Vegetationsgesellschaften unter Verwendung von multisensoralen UAS-Daten (Multitemporal evaluation of peatland vegetation communities using multisensoral UAS data). *gis.Science*, 4, 119–132 (in German).

Bivand, R., Keitt, T., Rowlingson, B. (2021) rgdal: bindings for the 'Geospatial' data abstraction library. Online at: https://CRAN.R-project.org/package=rgdal

Bonn, A., Allott, T., Evans, M., Joosten, H., Stoneman, R. (2016) Peatland restoration and ecosystem services: An introduction. In: Bonn, A., Allott, T., Evans, M., Joosten, H., Stoneman R. (eds.) *Peatland Restoration and Ecosystem Services: Science, Policy and Practice*, Cambridge University Press (UK), 1–16.

Breiman, L. (2001) Random Forests. *Machine Learning*, 45, 5–32.

Coops, H., van der Velde, G. (1995) Seed dispersal, germination and seedling growth of six helophyte species in relation to water-level zonation. *Freshwater Biology*, 34, 13–20.

Cunliffe, A.M., Assmann, J.J., Daskalova, G.N., Kerby, J.T., Myers-Smith, I.H. (2020) Aboveground biomass corresponds strongly with drone-derived canopy height but weakly with greenness (NDVI) in a shrub tundra landscape. *Environmental Research Letters*, 15, 125004, 15 pp.

Cunliffe, A.M., Anderson, K., Boschetti, F., Brazier, R.E. and 45 others (2022) Global application of an unoccupied aerial vehicle photogrammetry protocol for predicting aboveground biomass in non-forest ecosystems. *Remote Sensing in Ecology and Conservation*, 8, 57–71.

den Hartog, C., Segal, S. (1964) A new classification of the water-plant communities. *Acta Botanica*

Neerlandica, 13, 367–393.

Deutscher Wetterdienst (2023) Standort Teterow (Location Teterow) (in German). Online at: https://www.dwd.de/DE/leistungen/cdc/cdc_ueberblick-klimadaten.html?nn=16102

Dong, J., Kaufmann, R.K., Myneni, R.B., Tucker, C.J., Kauppi, P.E., Liski, J., Buermann, W., Alexeyev, V., Hughes, M.K. (2003) Remote sensing estimates of boreal and temperate forest woody biomass: carbon pools, sources, and sinks. *Remote Sensing of Environment*, 84, 393–410.

Doughty, C.L., Cavanaugh, K.C. (2019) Mapping coastal wetland biomass from high resolution unmanned aerial vehicle (UAV) imagery. *Remote Sensing*, 11, 540, 16 pp.

Doughty, C.L., Ambrose, R.F., Okin, G.S., Cavanaugh, K.C. (2021) Characterizing spatial variability in coastal wetland biomass across multiple scales using UAV and satellite imagery. *Remote Sensing in Ecology and Conservation*, 7, 411–429.

Erkens, G., van der Meulen, M.J., Middelkoop, H. (2016) Double trouble: subsidence and CO_2 respiration due to 1,000 years of Dutch coastal peatlands cultivation. *Hydrogeology Journal*, 24, 551–568.

Fassnacht, F.E., Poblete-Olivares, J., Rivero, L., Lopatin, J., Ceballos-Comisso, A., Galleguillos, M. (2021) Using Sentinel-2 and canopy height models to derive a landscape-level biomass map covering multiple vegetation types. *International Journal of Applied Earth Observation and Geoinformation*, 94, 102236, 12 pp.

Geipel, J., Link, J., Wirwahn, J.A., Claupein, W. (2016) A programmable aerial multispectral camera system for in-season crop biomass and nitrogen content estimation. *Agriculture*, 6, 4, 19 pp.

Geurts, J.J.M., Fritz, C. (2018) *Paludiculture Pilots and Experiments with Focus on Cattail and Reed in The Netherlands*. Technical Report, CINDERELLA project, Radboud University Nijmegen. Online at: https://www.researchgate.net/profile/Jeroen-Geurts-4/publication/326772321_Paludiculture_pilots_and_experiments_with_focus_on_cattail_and_reed_in_the_Netherlands/links/5b62bdb40f7e9bc79a751a6c/Paludiculture-pilots-and-experiments-with-focus-on-cattail-and-reed-in-the-Netherlands.pdf?origin=publication_detail, accessed 08 Nov 2023.

Geurts, J.J.M., Oehmke, C., Lambertini, C., Eller, F., Sorrell, B.K., Mandiola, S.R., Grootjans, A.P., Brix, H., Wichtmann, W., Lamers, L.P.M., Fritz, C. (2020) Nutrient removal potential and biomass production by *Phragmites australis* and *Typha latifolia* on European rewetted peat and mineral soils. *Science of the Total Environment*, 747, 141102, 10 pp.

Grace, J.B. (1988) The effects of nutrient additions on mixtures of *Typha latifolia* L. and *Typha domingensis* pers. along a water-depth gradient. *Aquatic Botany*, 31, 83–92.

Greifswald Mire Centre (2020a) Paludi-PRIMA. Online at: https://www.moorwissen.de/en/paludikultur/projekte/prima/index.php, accessed 19 Nov 2024.

Greifswald Mire Centre (2020b) Cultivation of Cattail (*Typha*) - pilot site 'Teichweide', Neukalen. Online at: https://www.moorwissen.de/en/paludikultur/imdetail/umsetzungsbeispiele/prima_demo/index.php, accessed 19 Nov 2024.

Grosshans, R.E. (2014) *Cattail (*Typha *spp.) Biomass Harvesting for Nutrient Capture and Sustainable Bionenergy for Integrated Watershed Management*. PhD thesis, University of Manitoba, Winnipeg, Canada, 292 pp.

Günther, A., Barthelmes, A., Huth, V., Joosten, H., Jurasinski, G., Koebsch, F., Couwenberg, J. (2020) Prompt rewetting of drained peatlands reduces climate warming despite methane emissions. *Nature Communications*, 11, 1644, 5 pp.

Heinz, S.I. (2011) *Population Biology of* Typha latifolia *L. and* Typha angustifolia *L.: Establishment, Growth and Reproduction in a Constructed Wetland*. Dissertation, Technische Universität München, Germany, 111 pp. Online at: https://mediatum.ub.tum.de/doc/1002251/1002251.pdf, accessed 08 Nov 2023.

Hijmans, R.J. (2022) terra: Spatial data analysis. Online at: https://CRAN.R-project.org/package=terra

Hübner, F. (2021) *Assessment of Growth Patterns of* Typha *spec. on a Paludiculture Pilot Scheme Using Spectral Measurements at Different Spatial Scales*. Master thesis, University of Greifswald, Germany, 92 pp.

Hunt, E.R., Cavigelli, M., Daughtry, C.S.T., Mcmurtrey, J.E., Walthall, C.L. (2005) Evaluation of digital photography from model aircraft for remote sensing of crop biomass and nitrogen status. *Precision Agriculture*, 6, 359–378.

Joosten, H. (2016) Peatlands across the globe. In: Bonn, A., Allott, T., Evans, M., Joosten, H., Stoneman, R. (eds.) *Peatland Restoration and Ecosystem Services: Science, Policy and Practice*, Cambridge University Press (UK), 19–43.

Klemas, V. (2013) Remote sensing of coastal wetland biomass: An overview. *Journal of Coastal Research*, 29, 1016–1028.

Liaw, A., Wiener, M. (2002) Classification and regression by randomForest. *R News*, 2, 18–22.

Lopatin, J., Kattenborn, T., Galleguillos, M., Perez-Quezada, J.F., Schmidtlein, S. (2019) Using

aboveground vegetation attributes as proxies for mapping peatland belowground carbon stocks. *Remote Sensing of Environment*, 231, 111217, 14 pp.

Lu, L., Luo, J., Xin, Y., Duan, H., Sun, Z., Qiu, Y., Xiao, Q. (2022) How can UAV contribute in satellite-based *Phragmites australis* aboveground biomass estimating? *International Journal of Applied Earth Observation and Geoinformation*, 114, 103024, 10 pp.

Luo, S., Wang, C., Xi, X., Pan, F., Qian, M., Peng, D., Nie, S., Qin, H., Lin, Y. (2017) Retrieving aboveground biomass of wetland *Phragmites australis* (common reed) using a combination of airborne discrete-return LiDAR and hyperspectral data. *International Journal of Applied Earth Observation and Geoinformation*, 58, 107–117.

Madec, S., Baret, F., de Solan, B., Thomas, S., Dutartre, D., Jezequel, S., Hemmerlé, M., Colombeau, G., Comar, A. (2017) High-throughput phenotyping of plant height: Comparing unmanned aerial vehicles and ground LiDAR estimates. *Frontiers in Plant Science*, 8, 2002, 14 pp.

Mutanga, O., Adam, E., Cho, M.A. (2012) High density biomass estimation for wetland vegetation using WorldView-2 imagery and random forest regression algorithm. *International Journal of Applied Earth Observation and Geoinformation*, 18, 399–406.

Närmann, F., Birr, F., Kaiser, M., Nerger, M., Luthardt, V., Zeitz, J., Tanneberger, F. (2021) *Klimaschonende, biodiversitätsfördernde Bewirtschaftung von Niedermoorböden* (*Climate Friendly, Biodiversity Promoting Management of Fen Peatlands*). BfN-Skripten 616, Bundesamt für Naturschutz, Bonn, 342 pp. (in German). Online at: https://bfn.bsz-bw.de/frontdoor/deliver/index/docId/1036/file/Skript616.pdf, accessed 19 Nov 2024.

Neubert, J., Köhn, N., Haldan, K., Kuprina, K., Wichmann, S. (2022) *Paludikultur in die Praxis bringen: Integration - Management - Anbau*. (*Putting Paludiculture into Practice: Integration - Management - Cultivation*). Final report on the Paludi-PRIMA project, Greifswald University (Förderkennzeichen 22026017), 82 pp. (in German). Online at: https://www.fnr.de/ftp/pdf/berichte/22026017.pdf, accessed 12 Nov 2024.

Oehmke, C., Abel, S. (2016) Ausgewählte Paludikulturen (Selected paludicultures). In: Wichtmann, W., Schröder, C., Joosten, H. (eds.) *Paludikultur - Bewirtschaftung nasser Moore* (*Paludiculture - Management of Wet Peatlands*), Schweizerbart Science Publishers, Stuttgart, Germany, 22–38 (in German).

Pätzig, M., Geiger, F., Rasche, D., Rauneker, P., Eltner, A. (2020) Allometric relationships for selected macrophytes of kettle holes in northeast Germany as a basis for efficient biomass estimation using unmanned aerial systems (UAS). *Aquatic Botany*, 162, 103202, 8 pp.

Pfadenhauer, J., Wild, U. (2001) Rohrkolbenanbau in Niedermooren - Integration von Rohstoffgewinnung, Wasserreinigung und Moorschutz zu einem nachhaltigen Nutzungskonzept (Cattail cultivation in fens - integration of raw material extraction, water purification and peatland protection into a sustainable utilisation concept). DBU website (Projects) (in German). Online at: https://www.dbu.de/projekt_10628/_db_1036.html, accessed 19 Nov 2024.

Pijlman, J., Geurst, J.J.M., Vroom, R., Bestman, M., Fritz, C., van Ekeren, N. (2019) The effects of harvest date and frequency on the yield, nutritional value and mineral content of the paludiculture crop cattail (*Typha latifolia* L.) in the first year after planting. *Mires and Peat*, 25, 04, 19 pp.

Poley, L.G., McDermid, G.J. (2020) A systematic review of the factors influencing the estimation of vegetation aboveground biomass using Unmanned Aerial Systems. *Remote Sensing*, 12, 1052, 46 pp.

QGIS Development Team (2021): QGIS Geographic Information System. QGIS Association. Online at: https://www.qgis.org

R Core Team (2022) *R: A Language and Environment for Statistical Computing: R Version 4.2.2*. The R Foundation, Vienna, Austria. Online at: https://www.R-project.org/

Räsänen, A., Juutinen, S., Aurela, M., Virtanen, T. (2019) Predicting aboveground biomass in Arctic landscapes using very high spatial resolution satellite imagery and field sampling. *International Journal of Remote Sensing*, 40, 1175–1199.

Räsänen, A., Juutinen, S., Kalacska, M., Aurela, M., Heikkinen, P., Mäenpää, K., Rimali, A., Virtanen, T. (2020) Peatland leaf-area index and biomass estimation with ultra-high resolution remote sensing. *GIScience & Remote Sensing*, 57, 943–964.

Räsänen, A., Wagner, J., Hugelius, G., Virtanen, T. (2021) Aboveground biomass patterns across treeless northern landscapes. *International Journal of Remote Sensing*, 42, 4536–4561.

Ren, L., Eller, F., Lambertini, C., Guo, W.-Y., Brix, H., Sorrell, B.K. (2019) Assessing nutrient responses and biomass quality for selection of appropriate paludiculture crops. *Science of the Total Environment*, 664, 1150–1161.

Sale, P.J.M., Wetzel, R.G. (1983) Growth and metabolism of *Typha* species in relation to cutting treatments. *Aquatic Botany*, 15, 321–334.

Schulz, K., Timmermann, T., Steffenhagen, P., Zerbe, S., Succow, M. (2011) The effect of

flooding on carbon and nutrient standing stocks of helophyte biomass in rewetted fens. *Hydrobiologia*, 674, 25–40.

Schwieger, S., Kreyling, J., Couwenberg, J., Smiljanić, M., Weigel, R., Wilmking, M., Blume-Werry, G. (2021) Wetter is better: Rewetting of minerotrophic peatlands increases plant production and moves them towards carbon sinks in a dry year. *Ecosystems*, 24, 1093–1109.

Seiler, S. (2021) *Impacts of Environmental Factors and Cultivation Parameters on the Establishment of* Typha latifolia *and* Typha angustifolia *at a Paludiculture Site*. Master thesis, University Greifswald, Germany, 67 pp.

Tanneberger, F., Tegetmeyer, C., Dylawerski, M., Flade, M., Joosten, H. (2009) Commercially cut reed as a new and sustainable habitat for the globally threatened Aquatic Warbler. *Biodiversity and Conservation*, 18, 1475–1489.

Tiemeyer, B., Albiac Borraz, E., Augustin, J., Bechtold, M. and 19 others (2016) High emissions of greenhouse gases from grasslands on peat and other organic soils. *Global Change Biology*, 22, 4134–4149.

Timmermann, T. (2003) Nutzungsmöglichkeiten der Röhrichte und Riede wiedervernässter Niedermoore Mecklenburg-Vorpommerns (Utilisation options for reeds and sedges of rewetted fens in Mecklenburg-Western Pomerania). *Greifswalder Geographische Arbeiten*, 31, 31–42 (in German).

Tucker, C.J. (1977) Asymptotic nature of grass canopy spectral reflectance. *Applied Optics*, 16, 1151–1156.

Uellendahl, K., Hirschelmann, S., Abel, S. (2023). *Treibhausgas-Emissionen der moorreichen Bundesländer und die Rolle der organischen Böden* (*Greenhouse Gas Emissions of the Federal States in Germany with Abundant Peatlands and the Role of Organic Soils*). Informationspapier, Greifswald Moor Centrum, 12 pp. (in German). Online at: https://greifswaldmoor.de/files/dokumente/Infopapiere_Briefings/202305_Faktenpapier%20Emissionen%20Bundesl%C3%A4nder_final%20_korr.pdf, accessed 19 Nov 2024.

Ullah, S., Si, Y., Schlerf, M., Skidmore, A.K., Shafique, M., Iqbal, I.A. (2012) Estimation of grassland biomass and nitrogen using MERIS data. *International Journal of Applied Earth Observation and Geoinformation*, 19, 196–204.

UNEP (2022) *Global Peatlands Assessment: The State of the World's Peatlands*. Main Report, United Nations Environment Programme (UNEP), Nairobi, 425 pp.

Vroom, R.J.E., Xie, F., Geurts, J.J.M., Chojnowska, A., Smolders, A.J.P., Lamers, L.P.M., Fritz, C. (2018) *Typha latifolia* paludiculture effectively improves water quality and reduces greenhouse gas emissions in rewetted peatlands. *Ecological Engineering*, 124, 88–98.

Wan, R., Wang, P., Wang, X., Yao, X., Dai, X. (2019) Mapping aboveground biomass of four typical vegetation types in the Poyang Lake Wetlands based on random forest modelling and Landsat images. *Frontiers in Plant Science*, 10, 1281, 14 pp.

Wang, C., Menenti, M., Stoll, M.-P., Feola, A., Belluco, E., Marani, M. (2009) Separation of ground and low vegetation signatures in LiDAR measurements of salt-marsh environments. *IEEE Transactions on Geoscience and Remote Sensing*, 47, 2014–2023.

Wichtmann, W., Joosten, H. (2007) Paludiculture: peat formation and renewable resources from rewetted peatlands. *IMCG Newsletter*, 2007/3, 24–28.

Wild, U., Kamp, T., Lenz, A., Heinz, S., Pfadenhauer, J. (2001) Cultivation of *Typha* spp. in constructed wetlands for peatland restoration. *Ecological Engineering*, 17, 49–54.

Willkomm, M., Bolten, A., Bareth, G. (2016) Non-destructive monitoring of rice by hyperspectral in-field spectrometry and UAV-based remote sensing: Case study of field-grown rice in North Rhine-Westphalia, Germany. *The International Archives of the Photogrammetry, Remote Sensing and Spatial Information Sciences*, XLI-B1, 1071–1077.

Zaidi, S.S.A., Ansari, M.S., Aslam, A., Kanwal, N., Asghar, M., Lee, B. (2022) A survey of modern deep learning based object detection models. *Digital Signal Processing*, 126, 103514, 19 pp.

Zak, D., Wagner, C., Payer, B., Augustin, J., Gelbrecht, J. (2010) Phosphorus mobilization in rewetted fens: the effect of altered peat properties and implications for their restoration. *Ecological Applications*, 20, 1336–1349.

Submitted 30 Nov 2023, revision 26 Sep 2024
Editor: Colin McCarter

Author for correspondence:
Christina Hellmann, Institute of Geography and Geology, University of Greifswald, partner in the Greifswald Mire Centre, Friedrich-Ludwig-Jahn-Str. 16, D-17489 Greifswald, Germany.
Tel: +49 3834 420 4544; Email: christina.hellmann@uni-greifswald.de